Composite of Polyaniline/Reduced Graphene Oxide with The Single-, Bi- and Tri- metal Oxides Modification and the Effect on the Capacitance Properties

Atmanto Heru Wibowo
Department of Chemistry, Sebelas Maret University

Husen Al Arraf
Department of Chemistry, Sebelas Maret University

Masykur, Abu
Department of Chemistry, Sebelas Maret University

Rahmawati, Fitria
Department of Chemistry, Sebelas Maret University

他

https://doi.org/10.5109/6781053

出版情報：Evergreen. 10 (1), pp.85-93, 2023-03. 九州大学グリーンテクノロジー研究教育センター
バージョン：

Composite of Polyaniline/Reduced Graphene Oxide with The Single-, Bi- and Tri- metal Oxides Modification and the Effect on the Capacitance Properties

Atmanto Heru Wibowo[1,*], Husen Al Arraf[1], Abu Masykur[1], Fitria Rahmawati[1], Maulidan Firdaus[1], Felix Pasila[2], Ulya Farahdina[3], and Nasori Nasori[3]

[1]Department of Chemistry, Sebelas Maret University, Jl. Ir. Sutami 36A, Surakarta, Indonesia

[2]Electrical Engineering Department, Petra Christian University, Surabaya, Indonesia

[3]Department of Physics, Faculty of Sciences and Data Analytic, Institut Teknologi Sepuluh November, Surabaya, Indonesia

*Author to whom correspondence should be addressed:
E-mail: aheruwibowo@staff.uns.ac.id

(Received October 27, 2022; Revised January 16, 2023; accepted March 17, 2023).

Abstract: The composites of polyaniline (PANI) with reduced graphene oxide (PANI/rGO) and metals of iron, copper, and cobalt have been synthesized and coated on the nickel foam (NF) priors to measurement in three electrodes system to investigate the electrochemical properties. Surface area of PANI increased from 48.371 m^2/g to 69.091 m^2/g after compositing with rGO and the capacitance changed from 246.50 F/g to the highest capacitance 285.89 F/g in the form of PANI/rGO-Cu. Meanwhile, PANI/rGO-Co and PANI/rGO-Fe showed lower capacitance with 250.047 F/g and 254.71 F/g, respectively. Capacitance of bi-and tri-metal content was lower than PANI.

Keywords: rGO; PANI; transition metals; composites; capacitance

1. Introduction

Nowadays, the development of carbon for special use and related synthesis in some fields have been significant increasing for decades. The studies of carbon materials in the use for such adsorption[1,2], catalyst support[3] and various synthesizes using such arc discharge[4] and electrospray deposition[5] have been reported. Carbons are also considered as one of potential materials due to its electrical and conductivity properties. Moreover, kinds of a super capacitor electrode material are theoretically divided into three types; carbon-based, conducting polymers and metal oxides[6]. In the further development, two or more components of materials above practically have been mixed in the seeking of appropriate electrochemical and mechanical properties. Recently, the wide-range organic polymer compounds have been increasingly used in the investigation of the development in composite material for electromagnetic and conducting or supporting-conducting materials. Like cellulose base composites have been used for as electroactive bio composite[7], ionic conductivity and ion exchange activity[8]. Fiber base materials such cotton[9], bamboo[10] curauá [11] have been reported in regards with mechanical, electromagnetic and antistatic reinforced properties. Among other conducting polymers, PANI has attracted more attention recently for the development of composite of materials electrodes and increasingly investigated from year to years due to high conductivity and excellent capacitive properties[12], synthesis ease and low cost production[13].

Nowadays, formulation of PANI base electrode related to conductivity and mechanical properties have been also directed in combination with two or more supporting materials, in example, silver-nano-wire/polyimide[14], bucky paper/polydivinylbenzene[15]. Carbon base structure such graphene[16], rGO[17], fullerene[6] as well as carbon nano tube (CNT) have been reported intensively as composite materials with PANI mostly in regards with thermoelectric properties[18,19], electrical conductivity[20,21] and their capacitance performance[16]. In the advance development, dopants of transition metals are also incorporated as they are able to serve as redox active catalysts, enhance the capacitance and increase the energy density[22]. NiO[23], MnO_2[24], and σ-Fe_2O_3[25] have been used in composite of PANI base electrodes as metal oxide dopants. Furthermore, two transition metal dopants in one composite PANI electrode have also been used by. Kathalingam, et. al. [26] in which these metals in the spinel structure synergistically enhance electrochemical performance. This strategy of mixing two different transition metal oxides can offer higher electronic

conductivity than single oxides in the PANI composite as it was in the use of iron/zinc dopants[27].

In this work, PANI/rGO composites are synthesized through hydrothermal reaction, and used as electrode materials on the nickel foam (NF). Single-, bi-, and tri-metal modification have been applied to PANI/rGO aim to increase their specific surface area (m^2/g), and their specific capacitance (F/g). Three different transition-metal oxides copper (Cu), cobalt (Co) and iron (Fe) have been used as modifiers. The produced-composites were then characterized to understand their specific diffraction peaks, the molecular vibrations, the specific-surface area (m^2/g), and their electrochemical activities within the alkaline solution under a different scan rate. Low concentration of potassium hydroxide (KOH) was used to avoid the limit of the cycle life of electrochemical capacitor and to avoid metal oxides to degrade dramatically in concentrated solutions[28]. The specific capacitance of single-metal dopants in the PANI/rGO composites are then compared with bimetal and trimetal oxides in the three-electrodes system with the produced-composite as working electrode, Pt as counter electrode, and Ag/AgCl as reference electrode. The cyclic-voltammogram was recorded under -0.6 to 0.3 V vs Ag/AgCl at different scan rate to investigate their capacitive performance.

2. Experimental Method

2.1 Materials

Graphite (3000 mesh) was bought for the synthesis of graphene oxide from Qingdao Furuite graphite (synthesis was done with Hummer method and not reported in this paper), 37% hydrochloric acid (HCl), copper sulfate pentahydrate ($CuSO_4.5H_2O$), cobalt sulfate heptahydrate ($CoSO_4.7H_2O$), iron sulfate heptahydrate ($FeSO_4.7H_2O$), aniline, ammonium persulfate $(NH_4)_2S_2O_8$ were from Sigma Aldrich. Acetylene black were from Zhengzhou Kelin Water Purification Material. Polyvinylidene fluoride (PVDF) was bought from Jinan Future Chemical. N-methyl pyrrolidone (NMP), nickel foam and aniline were from Richnow Chemical Industry.

2.2 Instruments

X-Ray Diffraction (Cu,Kα) with scan rate of 10°/minutes and angle of 3-90° from Expert Pan Analytical was used to identify graphite, GO, rGO, PANI and composites. Fourier Transform Infra-Red (FTIR) analyzer with scan rate 400-4000 cm^{-1} from Shimadzu type IR Prestige-21was used to characterize functional groups of materials and composites. Scanning Electron Microscopy (SEM) from FEI type Inspect S50 was used to investigate the surface of materials and composites. Surface Area Analyzer (SAA) from Nova Win Quantachrome tipe 1200e was used to measure the surface area and pore size of materials and composites. Cyclic Voltammetry from Wuhan CorrTest Electrochemical Workstation type CS350 was used to measure the electrochemical performance of electrode.

2.3 Procedures

2.3.1 Synthesis of Polyaniline (PANI)

Polyaniline (PANI) was synthesized by chemical oxidation-polymerization method. The PANI was synthesized by mixing of 4.5 mL aniline monomer in 70 mL hydrochloric acid with 4.5 g ammonium persulfate in 20 mL distilled water. The mixture was stirred and cooled in the ice bath for 3h. Green precipitate formed was filtered and washed with ethanol and distilled water. The product was dried to obtain PANI powder.

2.3.2 Synthesis of PANI/rGO/Metal Oxide

Synthesis of PANI/rGO/metal oxides composites were done by mixing 35 mg of GO in 10 mL of distilled water, 100 µL aniline monomer and 10 mL HCl 2M. Then, 200 mg ammonium persulfate in 10 mL of distilled water was added and stirred in ice bath for 3h followed by the addition of 10 mL of 0.1 M metal solutions ($CuSO_4.5H_2O$, $FeSO_4.7H_2O$, and $CoSO_4.7H_2O$) in distilled water and stirred at room temperature for 1h. Green precipitate formed was filtered and washed with distilled water followed by hydrothermal reaction for 12h at 180°C before drying with vacuum to obtain PANI/rGO/metal oxide powder.

2.3.3 Preparation of working electrode

Working electrode was fabricated by attachment of the PANI/rGO/metal on the nickel foam (NF) plate (1cm x 1cm x 1mm). NF was firstly washed by 0.1 M hydrochloric acid, methanol, acetone, and water respectively with sonication before dried at 60^0C overnight. Attachment of material on NF was done using the mixture of acetylene black and PVDF with mass ratio of 80%:10%:10%. These mixtures were dropped with a little NMP until paste form obtained. NF was then coated with paste until all surface covered. Paste-covered NF was dried in an oven at 60^0C for 12 h. Working electrodes were ready to use.

2.3.4 Cyclic Voltammetry (CV) Analysis

Three electrodes system of CV was used to investigate the electrochemical activities during forward and backward voltage scanning of -0.6 to 0.3 V. CV analysis also was used to understand the reversibility of the redox reaction, and the pseudo-capacitive performance of the electrode made. Ag/AgCl electrode was used as reference electrode. Meanwhile, 20 x 20 mm platina plate was used as counter electrode and PANI/rGO/metal composite coated on NF was used as working electrode. Measurement was done under -0.6 to 0.3 V with scanning rate of 5-100 mV/s and in 0.1 M potassium hydroxide solution. Specific capacity, *Cp* was determined from CV curve by applying equation (1).

$$Cp = \frac{\int I(V)dV}{k \,.\, m \,.\, \Delta V} \qquad (1)$$

In which $I\,dV$ is the area of voltammetric curve, m is mass of the prepared-material embedded to Ni foam (g), k is scanning rate (mVs^{-1}) and ΔV is potential window.

3. Result and Discussion

The objective of this study is to get advantage of the combination of rGO, PANI and various metal oxides from single, bi and trimetallic of different kind of transition metal contents (iron, copper, and cobalt) of this layered material on the NF. From the literature obtained, the comparison of the use of the three metals of iron, copper, and cobalt together with PANI and rGO, and also the synergistic effects of these metals towards the capacitance properties have not been reported before. However, the limitation of the study focuses on the gaining information from the change of the physical properties and electrochemical measurement obtained from some parameters, mainly surface area and also capacitance properties.

Carbonaceous materials are well known as non-faradaic groups such rGO with high surface area, and considered with good electrochemical conductivity, chemical stability and thermal stability. However, rGO has lower specific capacitance and energy density. The main reason is the agglomeration of rGO layers that cause the reducing the surface area of the native of rGO structure with the following consequence of the reduce of the capacitance. Theoretically, modification of rGO material with at least one of the conducting materials such PANI is one way to solve the problem of the use of rGO. Besides, metal oxides were also used to facilitate the transport and to increase ionic diffusion. Here, as the state art of the study, we combined more than one kind of metal oxides together with PANI and rGO onto the NF for an electrode and investigated the capacitance properties of this combination.

3.3 Synthesis of PANI/rGO and PANI/rGO/Metal composites

In this study, composites of PANI/rGO have been obtained by in-situ reaction of GO and aniline in the present of acid and ammonium persulfate. The similar procedure was also done for the synthesis of of PANI/rGO/metal oxide composite. The FTIR spectra of PANI/rGO composite product. Figure. 1 stated that the structure of rGO showed peak of OH residue at about 3450 cm^{-1} and CO at 1157 cm^{-1}. C=C and C=O stretching were seen at 1546 cm^{-1} (double peaks of symmetric and asymmetric) and 1720 cm^{-1}. Meanwhile, The PANI spectrum was showed with characteristic peaks from NH stretching at 3436 cm^{-1}, -C=C- benzenoid rings at 1555 and 1477 cm^{-1}, C–N aromatic amine at 1294 cm^{-1} and 1237 cm^{-1}, respectively. Due to the physical interaction between PANI and rGO, Peaks of PANI-rGO were as a combination between both compound that were seen as NH stretching, C=O, C=C aromatic. Some chemical shifting occurred due to the atom interactions such as electrostatic and hydrogen interaction in the PANI-rGO. The existence of quinoids ring in this compound was not seen.

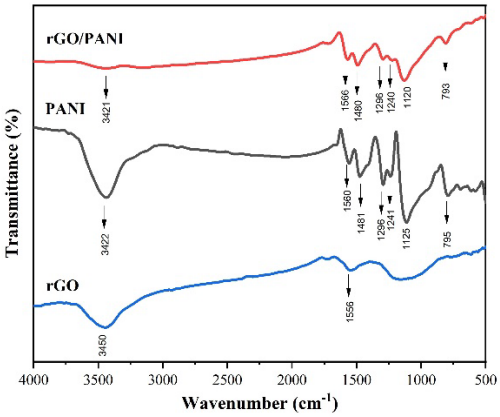

Fig. 1: FTIR spectra of rGO (blue line), PANI (black line) and PANI/rGO (red line).

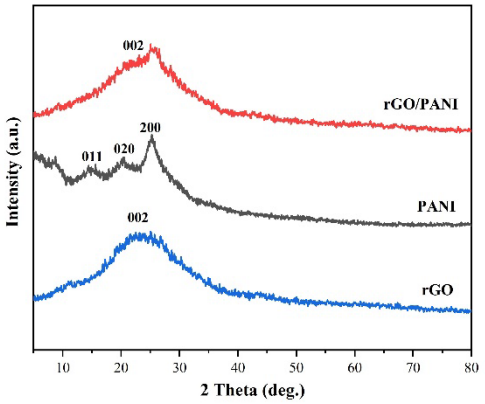

Fig. 2: Diffractogram of rGO (blue line), PANI (black line) and PANI/rGO (red line).

Diffractogram of rGO, PANI and PANI/rGO was showed in Figure 2. X-Ray diffraction of PANI (black line) showed 2Θ peaks at 15.2°, 20.9° and 25° indicated [011], [020] and [200] plane of crystal structure of emeraldine salt. rGO (blue line) showed peaks at 23.9° of [002] plane that was characteristic of rGO structure. Diffraction of PANI/rGO showed peaks that indicated PANI in the amorphous structure was weakly seen, due to low content of PANI in the composite. From the SEM data, it was also seen (in Figure 3) that surface morphology between rGO and PANI/rGO was different. PANI as organic polymer changed the surface of origin rGO from smooth with clear layer surface texture (see Figure 3a) to the disorder coarse layer due to agglomeration of PANI on the surface of rGO. (see Figure 3b).

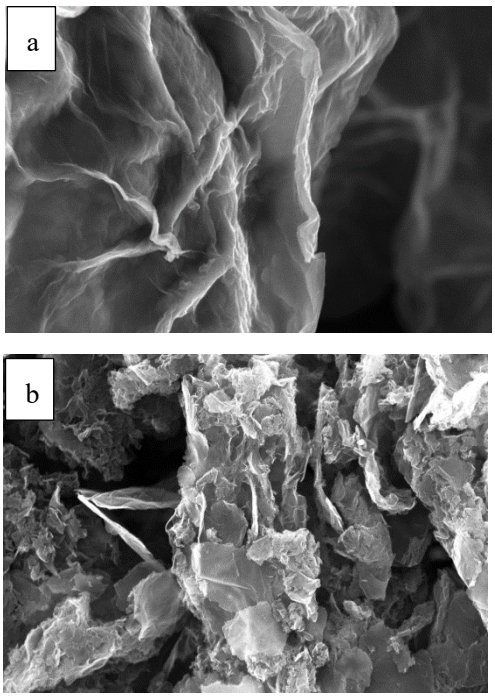

Fig. 3: Surface morphology of rGO (a) and PANI/rGO composite (b) with 5000 X magnificent.

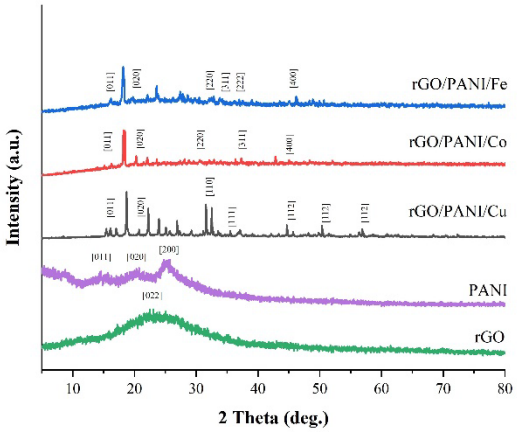

Fig. 4: X-Ray diffractogram of rGO (green line), PANI (purple line), PANI/rGO/Cu (black line), PANI/rGO/Co (red line), and PANI/rGO/Fe (blue line).

Figure 4. showed the X-Ray diffractogram of rGO/ PANI/metal of the synthesis product. Addition of transition metals in the PANI/rGO structure changed the diffraction pattern of the PANI/rGO origin composite, where peaks of metals present in the composites predominantly seen and raised more peaks of the origin one. Addition of copper in the PANI/rGO showed peaks at 32.5° [110], 35.5° [111], 46.3° [112], 51.3° [112], and 58.3° [202], in which this peak pattern indicated the formation of CuO (JCPDS 05-0661) in the composite after synthesis. Iron and cobalt oxide was also formed in the addition of iron and cobalt salt into the PANI/rGO. PANI/rGO/Co composite showed peaks at 31.2° [220], 36.8° [311], and 44.8° [400] of Co_3O_4 (JCPDS 42-1467). Meanwhile, PANI/rGO/Fe composite showed peak at 30.09° [220], 35.4° [311], 37.05° [222] and 43,05° [400] of Fe_3O_4 (JCPDS 19-0629).

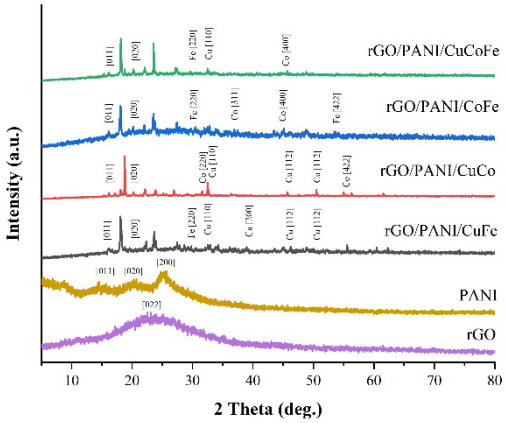

Fig. 5: X-Ray diffractogram of rGO, PANI, PANI/rGO/CuFe, PANI/rGO/CuCo, PANI/rGO/CoFe, and PANI/rGO/CuCoFe.

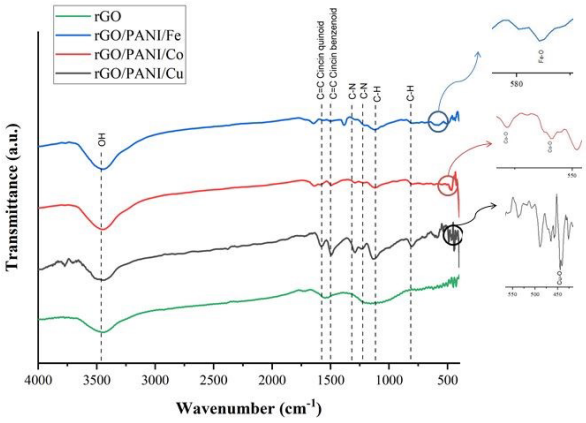

Fig. 6: FTIR spectra of composite with one metal content

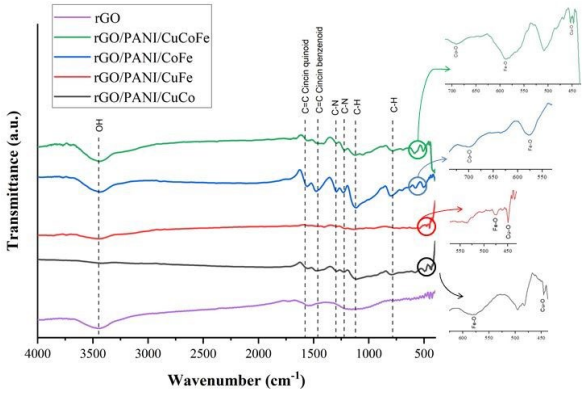

Fig 7: FTIR spectra of composite with bimetal and trimetal contents.

X-Ray diffractogram of PANI/rGO composite with various two and three metals content was showed in Figure 5. PANI/rGO/CuFe composite showed peaks of Fe_3O_4 and CuO and PANI/rGO/CuCo composite showed 2Θ peaks of Co_3O_4 and CuO. Meanwhile, peaks of Fe_3O_4 and Co_3O were seen in the PANI/rGO/CoFe. Peaks seen in the PANI/rGO/CuCoFe diffractogram represented the existence of Fe_3O_4, CuO and Co_3O_4. Meanwhile, FTIR

spectra of PANI/rGO/metal composites (Figure 6. and Figure 7.) showed predominantly characteristic vibrations of PANI and rGO. PANI/rGO/copper was seen at peak 445 cm^{-1} of Cu-O stretching, at 578 cm^{-1} and 559 cm^{-1} of the Co-O stretching of Co_3O_4 for PANI/rGO/Cobalt, and at 575 cm^{-1} of Fe-O stretching of Fe_3O_4 for PANI/rGO/iron. Meanwhile, three characteristic stretchings of Cu-O, Co-O and Fe-O were seen for the composite of PANI/rGO consist of iron, cobalt and copper. This result showed that PANI, besides as conducting polymers, also could act as the metal trapper and holder in the structure of composites.

3.4 Surface Area of Composites

Isotherm N_2 adsorption-desorption with BET method was used to investigate the effect of various metal modifier in the composites of PANI/rGO to the surface area and pore size. Figure 8. showed isotherm N_2 adsorption – desorption curve of PANI/rGO composites with various metal oxides. In general, the curves showed type IV of adsorption desorption pattern, such a typical mesopore material[29,30]. Meanwhile, loop hysteresis type H_3 indicated slit shape pore between composite layer[30,31]. Specific surface area and average porous diameter was showed on the Table 1.

Table 1 shows that the surface area of PANI is 48.371 m^2/g, and combining rGO with PANI has successfully increased the surface area to 69.09 m^2/g. It proves that rGO significantly contribute to the surface area increasing because of rGO itself provide a high surface area of 218.999 m^2/g. Cu modification to PANI/rGO even increased more the specific surface area to 98.076 m^2/g. This is in line with previous research by Carnes et al. [32] who found that Copper oxide has pores and tunnels that having ability to adsorb gas molecules.

Table 1. Comparison of surface area and average pore diameter.

Material	BET Surface Area (m^2/g)	Average Pore Diameter (nm)
rGO	218.999	3.844
PANI	48.371	3.376
PANI/rGO	69.091	3.794
PANI/rGO/Cu	98.076	3.798
PANI/rGO/Co	24.689	3.784
PANI/rGO/Fe	93.456	3.804
PANI/rGO/CuCo	26.198	3.790
PANI/rGO/CuFe	17.193	3.778
PANI/rGO/CoFe	29.805	3.376
PANI/rGO/CuCoFe	15.702	3.780

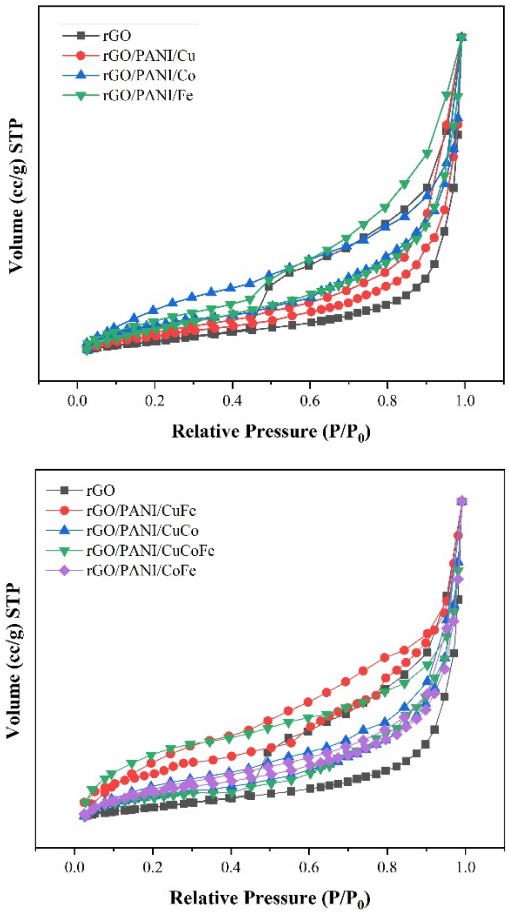

Fig. 8: Isotherm N_2 adsorption – desorption curve of PANI/rGO composites with single metallic (above) and bi and trimetallic (below).

3.5 Electrochemistry characterization

The correlation between electrochemical properties with physical properties of surface area, pore size, and also the dopant content in the composite was investigated from the voltammogram resulted in the measurement in the low concentration (0.1 M) of potassium hydroxide of the electrode. Electrochemical characterization of composite using three electrodes of *Cyclic Voltammetry* (CV) was showed in Figure 9. Voltammogram in Figure 9 shows anodic and cathodic peaks indicate a reversible redox reaction. The asymmetric form of the CV curve indicates Faradaic process of PANI which was started at around -0.0685 V with current density of 1.3945 x 10^{-5} A/cm^2 and cathodic peak at around -0.3796 V with current density of 2.7219 x 10^{-5} A/cm^2. Previous research on PANI substrat also found redox reaction of PANI which was defined as oxidation of leucomeraldine, the PANI form with semiconductor chacaracter, into *emeraldine* PANI. Meanwhile reduction reaction occurred from Emeraldine to Pernigraniline[33]. The specific capacitance of the prepared-materials are presented on the table 2.

Table 2 shows that the addition of rGO single metal increased surface area (m^2) of the material. The larger surface area allows more interaction between electrode material with the available cations and anions producing

higher capacity[34]. However, the addition of the metal dopants in the composite increased the reduction-oxidation reaction by the increasing sharpness of the anodic and cathodic peak at about -0,08 V and at about -0.39 V, where these sharp peaks were not seen on the PANI and rGO electrodes. The specific capacitance value was determined predominantly by the surface area of the composite (as seen in Figure 10) even though the metal composite dopant contents were able to facilitate increase the reduction-oxidation reaction in the electrodes. In this study, the proposed idea is to increase the conductivity of the PANI and rGO with various additional metals, from single, bi and trimetallic. Metal oxides were used to facilitate the transport and to increase ionic diffusion and also to increase the electrochemical activities. However, the capacitances obtained was lower than for instance the single PANI. It was due to the significant reduction of BET surface area after addition of single, bi and trimetallic compared to the single PANI 48.371 (as seen in Table 2). The surface area of the compound is the main factor for capacitance of the materials. It was stated by Ho et al.[28], the higher surface area can increase contact between the deposited active materials and electrolyte and then can enhance the capacitance.

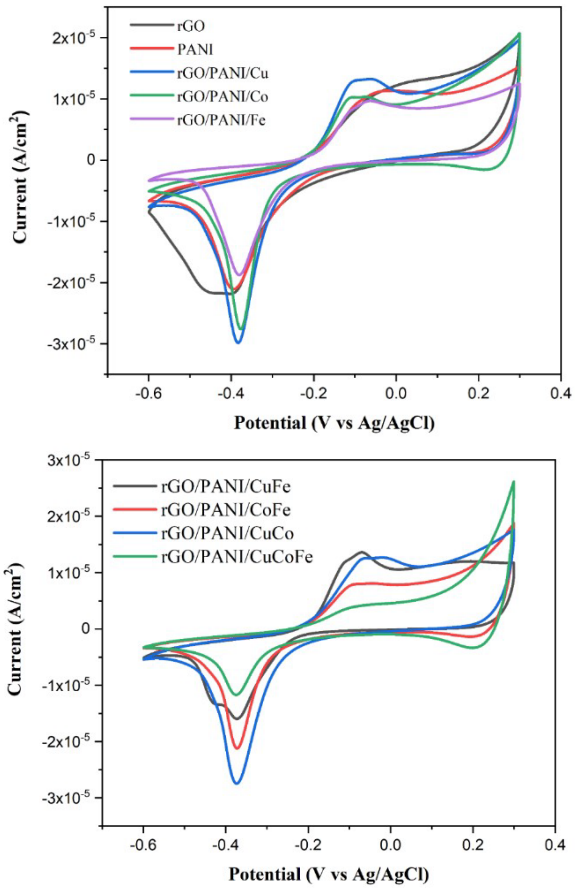

Fig. 9: Voltammogram of rGO and various PANI/rGO/metal oxide at scan rate 25 mV/s for single metal dopant content (above) and bi-and trimetallic dopant content (below).

Table 2. Specific capacitance of the prepared-materials.

Composite	Specific Capacitance (F/g)	Surface Area (m^2)
PANI	246.50	48.37
PANI/rGO/Cu	285.89	98.08
PANI/rGO/Co	250.05	24.69
PANI/rGO/Fe	254.71	93.46
PANI/rGO/CuCo	248.59	26.20
PANI/rGO/CuFe	211.14	17.19
PANI/rGO/CoFe	219.65	29.80
GO/PANI/CuCoFe	165.65	15.70

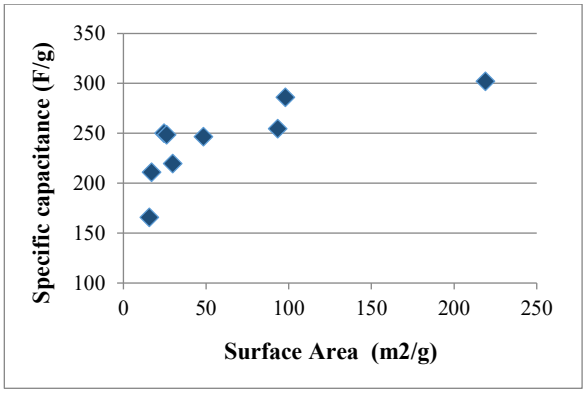

Fig. 10: Correlation between surface area and specific capacitance of composite.

The effect of variation of *scan rate* (5 – 100 mV/s) towards the specific capacitance was also determined in the composites made. The correlation was seen in the Figure 11. It was seen that the specific capacitance of the composite was affected by the scan rate of the measurements. The increase of the scan rate applied on the composite affected to the decrease of the specific capacitance. Capacitance and energy storage was influenced by the diffusion of the ions in the electrolyte. In the lower scan rate, hydroxyl ions in the electrolyte were enough time to reach the active site of the material electrode so as more ions were involved to contribute the increasing capacitance of the materials[35,36].

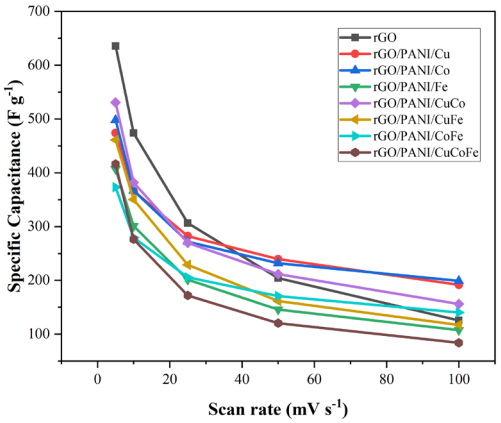

Fig. 11: Comparison curve of specific capacitance and scan rate.

Conclusion

Addition rGO-metal oxide into the PANI increased the surface area and the specific capacitance of the electrode. Among others, rGO/Cu showed the highest contribution to the increase of the specific capacitance from 245.50 F/g to 285.89 F/g. However, the addition of rGO along with bi- and tri-metals seems to provide nonproductive effect by decreasing surface area and specific capacitance. Therefore, composite of PANI with single rGO-metal is more reliable than bi- and tri-metal addition.

Acknowledgments

This project was funded by Ministry of Education, Research and Technology of Republic Indonesia and Sebelas Maret University

Nomenclature

Cp	specific capacity (F/g)
m	mass of the prepared-material (g)
k	scanning rate (mVs^{-1})
ΔV	potential window (V)

References

1) Chairunnisa, K. Thu, T. Miyazaki, K. Nakabayashi, J. Miyawaki, A. T. Wijayanta, and F. Rahmawati, "Highly microporous activated carbon from acorn nutshells and its performance in water vapor adsorption," *Evergreen*, **8** (*1*) 249–254 (2021). doi:10.5109/4372285.
2) Arikasuci Fitonna Ridassepri, F. Rahmawati, Kinkind Raras Heliani, Chairunnisa, J. Miyawaki, and Agung Tri Wijayanta, "Activated carbon from bagasse and its application for water vapor adsorption," *Evergreen*, **7** (*3*) 409–416 (2020). doi:10.5109/4068621.
3) F. Taufany, Mathilda Jowito Pasaribu, Berlina Yunita Sari Romaji, Y. Rahmawati, A. Altway, Susianto, S. Nurkhamidah, Julfikar Gilang Anfias, Y. Mursidah, F. Desi, S. Yulianti, D. Rahmawati, and G. Stellarosari, "The synthesis of activated carbon from waste tyre as fuel cell catalyst support," *Evergreen*, **9** (*2*) 412–420 (2022). doi:10.5109/4794166.
4) Isya Fitri Andhika, Teguh Endah Saraswati, and S. Hastuti, "The structural characteristics of carbon nanoparticles produced by arc discharge in toluene without added catalyst or gases," *Evergreen*, **7** (*3*) 417–428 (2020). doi:10.5109/4068622.
5) Muhammad Razlan Zakaria, Mohd Firdaus Omar, Hazizan Md Akil, and Mohd Mustafa Al Bakri Abdullah, "Study of carbon nanotubes stability in different types of solvents for electrospray deposition method," *Evergreen*, **7** (*4*) 538–543 (2020). doi:10.5109/4150473.
6) A. Ramadan, M. Anas, S. Ebrahim, M. Soliman, and A.I. Abou-Aly, "Polyaniline/fullerene derivative nanocomposite for highly efficient supercapacitor electrode," *International Journal of Hydrogen Energy*, **45** (*32*) 16254–16265 (2020). doi:10.1016/j.ijhydene.2020.04.093.
7) C.-H. Hong, S.-J. Ki, J.-H. Jeon, H. Che, I.-K. Park, C.-D. Kee, and I.-K. Oh, "Electroactive bio-composite actuators based on cellulose acetate nanofibers with specially chopped polyaniline nanoparticles through electrospinning," *Composites Science and Technology*, **87** 135–141 (2013). doi:10.1016/j.compscitech.2013.08.006.
8) L. Yue, Y. Xie, Y. Zheng, W. He, S. Guo, Y. Sun, T. Zhang, and S. Liu, "Sulfonated bacterial cellulose/polyaniline composite membrane for use as gel polymer electrolyte," *Composites Science and Technology*, **145** 122–131 (2017). doi:10.1016/j.compscitech.2017.04.002.
9) W. Zhang, X. Zhang, Z. Wu, K. Abdurahman, Y. Cao, H. Duan, and D. Jia, "Mechanical, electromagnetic shielding and gas sensing properties of flexible cotton fiber/polyaniline composites," *Composites Science and Technology*, **188** 107966 (2020). doi:10.1016/j.compscitech.2019.107966.
10) Z. Yang, Y. Zhang, and B. Wen, "Enhanced electromagnetic interference shielding capability in bamboo fiber@polyaniline composites through microwave reflection cavity design," *Composites Science and Technology*, **178** 41–49 (2019). doi:10.1016/j.compscitech.2019.04.023.
11) J.R. Araujo, C.B. Adamo, E. De Robertis, A.Yu. Kuznetsov, B.S. Archanjo, B. Fragneaud, C.A. Achete, and M.-A. De Paoli, "Crystallinity, oxidation states and morphology of polyaniline coated curauá fibers in polyamide-6 composites," *Composites Science and Technology*, **88** 106–112 (2013). doi:10.1016/j.compscitech.2013.08.039.
12) H. Wang, J. Lin, and Z.X. Shen, "Polyaniline (pani) based electrode materials for energy storage and conversion," *Journal of Science: Advanced Materials and Devices*, **1** (*3*) 225–255 (2016). doi:10.1016/j.jsamd.2016.08.001.
13) D. Salinas-Torres, J.M. Sieben, D. Lozano-Castelló, D. Cazorla-Amorós, and E. Morallón, "Asymmetric hybrid capacitors based on activated carbon and activated carbon fibre–pani electrodes," *Electrochimica Acta*, **89** 326–333 (2013). doi:10.1016/j.electacta.2012.11.039.
14) F. Fang, G.-W. Huang, H.-M. Xiao, Y.-Q. Li, N. Hu, and S.-Y. Fu, "Largely enhanced electrical conductivity of layer-structured silver nanowire/polyimide composite films by polyaniline," *Composites Science and Technology*, **156** 144–150 (2018). doi:10.1016/j.compscitech.2018.01.001.
15) X. Cheng, T. Yokozeki, H. Wang, L. Wu, and Q.-F. Sun, "Simultaneous enhancement of electrical conductivity and mechanical properties in buckypaper-reinforced polydivinylbenzene(doped polyaniline) composites," *Composites Science and*

Technology, **161** 50–56 (2018). doi:10.1016/j.compscitech.2018.03.042.
16) H. Yu, G. Xin, X. Ge, C. Bulin, R. Li, R. Xing, and B. Zhang, "Porous graphene-polyaniline nanoarrays composite with enhanced interface bonding and electrochemical performance," *Composites Science and Technology*, **154** 76–84 (2018). doi:10.1016/j.compscitech.2017.11.010.
17) J. Wang, B. Li, T. Ni, T. Dai, and Y. Lu, "One-step synthesis of iodine doped polyaniline-reduced graphene oxide composite hydrogel with high capacitive properties," *Composites Science and Technology*, **109** 12–17 (2015). doi:10.1016/j.compscitech.2015.01.008.
18) H. Li, Y. Liang, Y. Liu, S. Liu, P. Li, and C. He, "Engineering doping level for enhanced thermoelectric performance of carbon nanotubes/polyaniline composites," *Composites Science and Technology*, **210** 108797 (2021). doi:10.1016/j.compscitech.2021.108797.
19) P. Li, Y. Zhao, H. Li, S. Liu, Y. Liang, X. Cheng, and C. He, "Facile green strategy for improving thermoelectric performance of carbon nanotube/polyaniline composites by ethanol treatment," *Composites Science and Technology*, **189** 108023 (2020). doi:10.1016/j.compscitech.2020.108023.
20) C. Liu, I. Sergeichev, I. Akhatov, and K. Lafdi, "CNT and polyaniline based sensors for the detection of acid penetration in polymer composite," *Composites Science and Technology*, **159** 111–118 (2018). doi:10.1016/j.compscitech.2018.02.028.
21) Q. Qian, Y. Wang, M. Zhang, L. Chen, J. Feng, Y. Wang, and Y. Zhou, "Ultrasensitive paper-based polyaniline/graphene composite strain sensor for sign language expression," *Composites Science and Technology*, **181** 107660 (2019). doi:10.1016/j.compscitech.2019.05.017.
22) S. Dhibar, P. Bhattacharya, G. Hatui, S. Sahoo, and C.K. Das, "Transition metal-doped polyaniline/single-walled carbon nanotubes nanocomposites: efficient electrode material for high performance supercapacitors," *ACS Sustainable Chem. Eng.*, **2** (*5*) 1114–1127 (2014). doi:10.1021/ sc5000072.
23) Y. Wang, J. Guo, T. Wang, J. Shao, D. Wang, and Y.-W. Yang, "Mesoporous transition metal oxides for supercapacitors," *Nanomaterials*, **5** (*4*) 1667–1689 (2015). doi:10.3390/nano5041667.
24) P.H. Wadekar, R.V. Khose, D.A. Pethsangave, and S. Some, "One-step preparation of conducting polymer/metal oxide doped rgo trinary composite for supercapacitor applications," *ChemistrySelect*, **5** (*38*) 11769–11777 (2020). doi:10.1002/slct.202002911.
25) X.-F. Lu, X.-Y. Chen, W. Zhou, Y.-X. Tong, and G.-R. Li, "α-fe2o3@pani core–shell nanowire arrays as negative electrodes for asymmetric supercapacitors," *ACS Appl. Mater. Interfaces*, **7** (*27*) 14843–14850 (2015). doi:10.1021/acsami.5b03126.
26) A. Kathalingam, S. Ramesh, H.M. Yadav, J.-H. Choi, H.S. Kim, and H.-S. Kim, "Nanosheet-like znco2o4@nitrogen doped graphene oxide/polyaniline composite for supercapacitor application: effect of polyaniline incorporation," *Journal of Alloys and Compounds*, **830** 154734 (2020). doi:10.1016/j.jallcom.2020.154734.
27) P. Asen, S. Shahrokhian, and A.I. Zad, "Transition metal ions-doped polyaniline/graphene oxide nanostructure as high performance electrode for supercapacitor applications," *J Solid State Electrochem*, **22** (*4*) 983–996 (2018). doi:10.1007/s10008-017-3831-9.
28) M.Y. Ho, P.S. Khiew, D. Isa, T.K. Tan, W.S. Chiu, and C.H. Chia, "A review of metal oxide composite electrode materials for electrochemical capacitors," *NANO*, **09** (*06*) 1430002 (2014). doi:10.1142/S1793292014300023.
29) A. Bahadur, S. Iqbal, M. Shoaib, and A. Saeed, "Electrochemical study of specially designed graphene-fe3o4-polyaniline nanocomposite as a high-performance anode for lithium-ion battery," *Dalton Trans.*, **47** (*42*) 15031–15037 (2018). doi:10.1039/C8DT03107J.
30) X. Qiao, S. Liao, C. You, and R. Chen, "Phosphorus and nitrogen dual doped and simultaneously reduced graphene oxide with high surface area as efficient metal-free electrocatalyst for oxygen reduction," *Catalysts*, **5** (*2*) 981–991 (2015). doi:10.3390/catal5020981.
31) J.B. Condon, "Surface Area and Porosity Determinations by Physisorption: Measurement, Classical Theories and Quantum Theory," Elsevier, 2019.
32) C.L. Carnes, J. Stipp, K.J. Klabunde, and J. Bonevich, "Synthesis, characterization, and adsorption studies of nanocrystalline copper oxide and nickel oxide," *Langmuir*, **18** (*4*) 1352–1359 (2002). doi:10.1021/la010701p.
33) A. Viswanathan, and A.N. Shetty, "Facile in-situ single step chemical synthesis of reduced graphene oxide-copper oxide-polyaniline nanocomposite and its electrochemical performance for supercapacitor application," *Electrochimica Acta*, **257** 483–493 (2017). doi:10.1016/j.electacta.2017.10.099.
34) T. Ariyanto, I. Prasetyo, and R. Rochmadi, "PENGARUH struktur pori terhadap kapasitansi elektroda superkapasitor yang dibuat dari karbon nanopori," *Reaktor*, **14** (*1*) 25–32 (2012). doi:10.14710/reaktor.14.1.25-32.
35) N. Elgrishi, K.J. Rountree, B.D. McCarthy, E.S. Rountree, T.T. Eisenhart, and J.L. Dempsey, "A practical beginner's guide to cyclic voltammetry," *J. Chem. Educ.*, **95** (*2*) 197–206 (2018). doi:10.1021/acs.jchemed.7b00361.
36) M. Khalaj, A. Sedghi, H.N. Miankushki, and S.Z.

Golkhatmi, “Synthesis of novel graphene/co3o4/ polypyrrole ternary nanocomposites as electrochemically enhanced supercapacitor electrodes,” *Energy*, **188** 116088 (2019). doi:10.1016 /j.energy.2019.116088.